Systematic Study of the Structure–Property Relationships of Branched Hierarchical TiO2/ZnO Nanostructures

ARTICLE *in* ACS APPLIED MATERIALS & INTERFACES · NOVEMBER 2012

Impact Factor: 6.72 · DOI: 10.1021/am302061z · Source: PubMed

ACS APPLIED MATERIALS & INTERFACES

Research Article

www.acsami.org

Systematic Study of the Structure–Property Relationships of Branched Hierarchical TiO_2/ZnO Nanostructures

Thushara J. Athauda, Jonathan G. Neff, Logan Sutherlin, Umaiz Butt, and Ruya R. Ozer*

Department Chemistry and Biochemistry, University of Tulsa, 800 South Tucker Drive, Tulsa, Oklahoma 74104, United States

Supporting Information

ABSTRACT: We report a simple and effective route for fabricating branched hierarchical nanostructures of TiO_2/ZnO by combining electrospinning and the low-temperature hydrothermal growth technique. First, TiO_2 nanofibers were prepared by electrospinning polystyrene (PS)/titanium tetraisopropoxide ($Ti(OiPr)_4$) solutions onto glass substrates followed by calcination at 500 °C. The electrospun TiO_2 nanofibers served as a 3D primary platform upon which the branched, highly uniform, and dense secondary ZnO nanorods were hydrothermally grown. We observed that the concentration of $Ti(OiPr)_4$ in the polystyrene solution has a significant effect on the surface roughness and areal material ratio of the electrospun fibers. Most significantly, the morphology of the branched secondary ZnO nanorods and the overall charge transfer capacity of the nanoheterostructured systems are controlled by the density of the TiO_2 platform. This study demonstrates that, by properly choosing the synthesis parameters, it is possible to fine-tune the microscopic and macroscopic properties of branched hierarchical metal-oxide systems. The presented approach can be applied to the development of controlled, reproducible, miniaturized, and robust high-performance metal-oxide photovoltaic and photocatalytic systems.

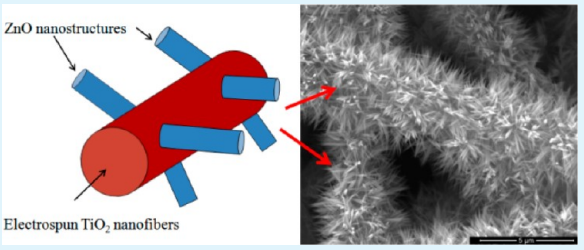

KEYWORDS: *electrospinning, nanofibers, nanorods, metal-oxide, TiO_2, ZnO, hydrothermal growth*

INTRODUCTION

Metal-oxide nanowires are considered to be synthetically tunable nanoscale building blocks for next-generation electronic devices and functional systems due to the quantum confinement effects in the radial axis, large aspect ratio, single-crystal properties, explicit control over composition and structure, and the directional mobility of charge carriers.[1−8] Heterostructures of metal-oxide nanowires, in which the secondary component grows in a radial or axial direction from a primary nanowire backbone, exhibit superior performances compared to single-component materials. These heterostructures can be tailored by fine-tuning the size, shape, composition, and organization pattern of the two or more nanoscale building blocks.[9−15] Enhancing the properties or multifunctionality of nanowire heterostructures would enable their use in electronics, photonics, catalysis, and sensing applications. In particular, because the nanoscale dimensions relax the lattice matching requirements, epitaxial crystal growth between dissimilar materials becomes feasible, which results in high-quality and defect-free junctions that can greatly enhance the charge transfer efficiency; this would be impossible in bulk films. Therefore, the overall device performance does not significantly suffer if lower quality materials are used, which allows significant cost reduction.

Electrospinning has become one of the most powerful techniques for fabricating nanorods, nanowires, and nanofibers due to its simplicity and low-cost and its ability to generate nanofibers that have small and uniform diameters, large specific surface areas, relatively smooth surfaces, and a high degree of structural order.[16−33] The electrospinning process uses electrostatic attraction generated by the high voltage between a charged polymer and a grounded collector to produce fine fibers that range in diameter from less than 10 nm to several micrometers. The fibers obtained using electrospinning usually possess a circular cross section. However, individual metal-oxides are not spinnable; that is, they need to be mixed, either as their sol–gel precursor or as nanoparticles, with a spinnable "carrier polymer". After calcination at high temperatures, metal-oxide nanofibers that have uniform dimensions and crystallinity can be obtained.[34−40] The electrospun metal-oxide nanofibers have been shown to possess faster electron transfer kinetics and better electrochemical properties than their cast films.[41−47] For example, the photoconversion efficiency and electron diffusion coefficient of electrospun TiO_2 nanowires were observed to be greater than that of flat films.[41,42] Electrospun TiO_2 nanofibers also exhibited greater photocatalytic activity for the decomposition of various dyes compared to bulk TiO_2.[41−44]

Composites of one or more metal-oxides can also be obtained by electrospinning. These metal-oxide composites can achieve very different electronic, mechanical, thermal, and optical properties than their constituent components, which can result in more versatile functions than individual materials when used for nanoscale devices.[48−53] Typically, sol–gel precursors of two or more metal-oxides are physically mixed

Received: September 21, 2012
Accepted: November 23, 2012
Published: November 23, 2012

with the carrier polymer followed by calcination. Electrospun composites of ZnO/SnO_2,[54] ZnO/TiO_2,[55,56] Zn/GeO_2,[57] NiO/SnO_2,[58] In_2O_3/TiO_2,[59] TiO_2/CdS,[60] and NiO/ZnO[61] have been shown to possess enhanced electrochemical activities. However, there is no control over the interfaces and/or prevention of alloy formation by mixing two or more metal-oxide precursors before electrospinning, which precludes predicting the final functionality of the material. However, greater control over the molecular properties can be obtained by designing arrayed heterostructures, in which the secondary structure is vertically branched or grown along the entire length of the primary structure. These arrayed heterostructures have been shown to possess superior or new functional properties compared to their individual constituents.[49−53] In particular, the electrospinning of primary structures followed by the hydrothermal growth of secondary structures provides an easy and inexpensive approach to the epitaxial growth of branched hierarchical heteronanostructures. For instance, ZnO/ZnO,[62] ZnO/TiO_2,[63] V_2O_5/TiO_2,[64] SnO_2/TiO_2,[65] and TiO_2/TiO_2[66] in the form of nanorods/nanofiber hierarchical heteronanostructures have been reported. The increased photocatalytic activity was considered to be an indication of the higher mobility of charge carriers due to the enhanced quality of the heterojunctions.

Here, we report a systematic study on the structure−property relationships of a branched hierarchical system of ZnO nanorods that were radially grown on electrospun TiO_2 nanofibers. The TiO_2/ZnO branched hierarchical nanostructures were identified as being the ideal system for exploring the size and dimensionality dependence of the structural, electronic, and optical properties, upon which more advanced complex metal-oxide systems can be developed. To date, there have been no reports on the effects of the structure on the surface resistivity of branched hierarchical metal-oxide nanostructures produced using the unique combination of electrospinning and the hydrothermal growth method. We also provide the first demonstration that the morphology of the primary electrospun nanofiber platform determines the shape of the radially grown secondary structures.

The general synthesis route for preparing branched hierarchical systems involves the following: (1) preparation of polymer solutions that contain the metal-oxide precursor, (2) electrospinning of the polymeric solution, (3) calcination of the electrospun nanofibers to generate metal-oxide structures by thermally removing the carrier polymer, and (4) hydrothermal growth of secondary branched nanorods on the metal-oxide nanofibers. The hydrothermal growth process requires two steps of seeding and growth treatments, which are performed in liquids, generally water, resulting in epitaxial and anisotropic crystal growth.[67−71]

In this study, a batch of TiO_2 nanofibers were prepared by electrospinning polystyrene (PS)/titanium tetraisopropoxide ($Ti(OiPr)_4$) solutions with different concentrations onto glass substrates followed by calcination at 500 °C. We observed that the concentration of titanium tetraisopropoxide in the electrospinning solution has a significant effect on the surface roughness and areal material ratio of the electrospun fibers. Next, the electrospun TiO_2 nanofibers were seeded with ZnO nanosols from an equimolar solution of zinc acetate and triethylamine in isopropyl alcohol. These ZnO nucleation sites lower the thermodynamic barrier, which consequently enable further growth of high aspect ratio ZnO nanorods in a solution of zinc nitrate and hexamethylenetetramine under relatively mild conditions. The experimental results revealed that the morphology of the branched secondary ZnO nanorods and the overall charge transfer capacity of the branched nanoheterostructured systems are controlled by the density of the primary electrospun TiO_2 platforms. This study demonstrates that, by properly choosing the synthesis parameters, it is possible to fine-tune the microscopic and macroscopic properties of branched hierarchical metal-oxide systems. The presented approach can be applied to the development of controlled and reproducible high-performance, miniaturized, and robust metal-oxide photovoltaic and photocatalytic systems.

EXPERIMENTAL SECTION

Chemicals and Materials. Polystyrene (PS) ($M_w \approx 280\,000$ Da), dimethyl formamide (DMF, anhydrous, 99.8%), titanium tetraisopropoxide ($Ti(OiPr)_4$, 97%), zinc acetate dihydrate ($Zn(CH_3COO)_2{\cdot}2H_2O$, ACS reagent, ≥98%), triethylamine ($(C_2H_5)_3N$, ≥99.5%), isopropyl alcohol (anhydrous, 99.5%), ethanol (ACS reagent, ≥99.5%, 200 proof, absolute), zinc nitrate hexahydrate ($Zn(NO_3){\cdot}6H_2O$, reagent grade 98%), and hexamethylenetetramine ($C_6H_{12}N_4$, ACS reagent, ≥99.0%) were purchased from Sigma-Aldrich. Premium microscope glass slides were purchased from Fisher Scientific.

Cleaning of Glass Slides: The glass slides were sonicated in deionized (DI) water and ethanol for 30 min each. The slides were then rinsed with DI water and dried in air.

Preparation of Electrospinning Solutions of Ti(OiPr)$_4$/PS: A 20 wt % PS stock solution was prepared in DMF by magnetic stirring in a 20 mL capped vial for 24 h. In a typical electrospinning procedure, the TiO_2 precursor, $Ti(OiPr)_4$, was mixed with the 20 wt % PS stock solution in certain proportions in a glovebox followed by vigorous stirring for 1 h for complete mixing. The $Ti(OiPr)_4$/PS solutions were prepared in a glovebox to prevent the hydrolysis of $Ti(OiPr)_4$ before electrospinning. The weight ratio of ($Ti(OiPr)_4$) in the PS solution was changed from 0 to 25 wt %. Fresh electrospinning solutions were prepared before each experiment.

Electrospinning Process: An aliquot of the freshly prepared $Ti(OiPr)_4$/PS solution was loaded into a 10 mL plastic syringe that was equipped with a blunt 18 gauge stainless steel needle. A Gamma High Voltage Research Power Supply that can generate up to 30 kV dc voltage was attached to the tip of the needle, which was placed in a syringe pump. The aluminum collector was placed 15 cm away from the tip of the needle and was attached to the grounding electrode. Typical spinning parameters were as follows: applied voltage was 10 kV; flow rate of the syringe pump was 20 μL/min; and the electrospinning duration was 20 min. The electrospun fibers were collected onto glass slides. For comparison purposes, the 20 wt % PS solution was also electrospun under identical conditions. The samples were then heated in an oven at 80 °C for complete removal of the solvent and condensation of TiO_2 before further analyses.

The glass slides were attached to the aluminum collector plate using tape, and the collector plate was supported by a stand. Due to the poor adhesion of the electrospun fibers to the glass slide, the samples were hot-pressed at 120 °C to ensure durable attachment to the surface. A 1 mm thick Teflon sheet was placed between the fibers and the plate to prevent them from sticking to the plate. The electrospun fibers were calcined at 500 °C for 90 min to remove the carrier polymer before the ZnO nanorods were grown.

Preparation of ZnO Seed Solution: Zinc acetate dehydrate (0.1 M, 1.0975 g) was dissolved in 50 mL of isopropyl alcohol, and the solution was vigorously stirred at 85 °C for 15 min. Then, 0.1 M triethylamine was added dropwise, which resulted in a clear solution. The reaction was maintained at that temperature for an additional 10 min and then aged at room temperature for 3 h (pH of the seed solution = 7.01). The resulting nanoparticles are spherical and stable for at least 2 weeks in solution. Initial deposition of the ZnO nanoparticles is critical for the formation of hexagonal ZnO nanorods

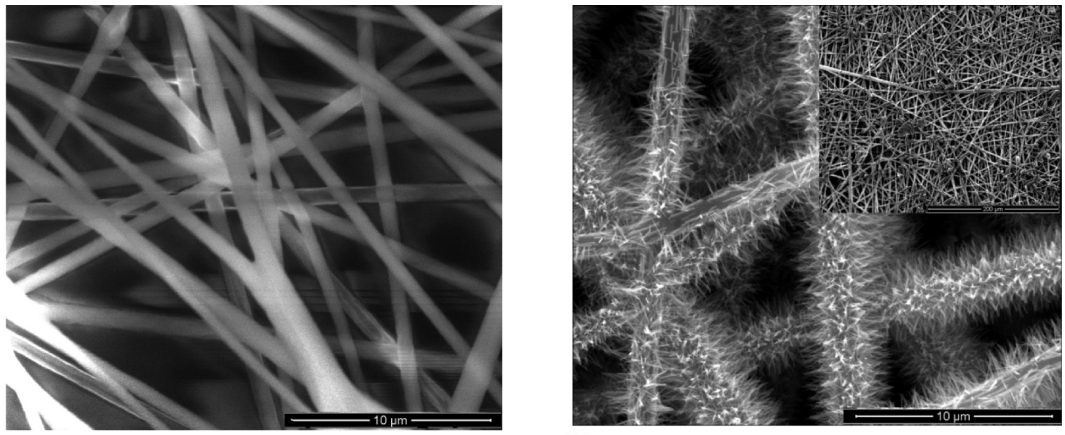

Figure 1. SEM images of (a) nanofibers electrospun from 20 wt % polystyrene solution, (b) ZnO nanorods hydrothermally grown on the nanofibers electrospun from 20 wt % polystyrene solution (inset: identical sample at low magnification).

Table 1. Physical Properties of the Electrospinning Solutions and the Electrospun Nanofibers

sample	$Ti(OiPr)_4$ wt % in electrospinning solution	TiO_2 wt % in electrospun fibers (TGA)	surface roughness (S_a) (μm) (±0.1)	areal material ratio (%) (±0.1)	average diameter (μm) (before calcination) (±0.01)
PS stock solution	0	0	33.3	66.3	7.0
sample 1	5.0	16.6	29.8	62.4	2.0
sample 2	10	16.9	23.5	59.1	1.7
sample 3	15	19.4	18.6	54.3	1.3
sample 4	20	26.2	15.3	47.8	1.1
sample 5	25	29.1	11.9	33.5	0.7

arranged vertically to the substrate surface. The deposited nanoparticles would be able to provide a large number of nucleation sites for the subsequent growth of the ZnO nanorods. The average particle size of the ZnO nanocrystal seed solution (0.1 M) was ~31.5 ± 10.0 nm, as measured by a Zetatrack (Microtrac) particle size analyzer.

Preparation of ZnO Growth Solution: Equimolar aqueous solutions of zinc nitrate hexahydrate and hexamethylenetetramine were used to grow the ZnO nanorods. First, 0.025 M hexamethylenetetramine (1.928 g) was prepared in 550 mL of DI water. Once completely dissolved, 0.025 M (4.090 g) of zinc nitrate hexahydrate was added to this solution, which was followed by stirring for 24 h (pH of the growth solution = 6.11).

Growth of ZnO Nanostructures on Electrospun Nanofibers: The electrospun nanofibers were first dip-coated with the seed solution for 5 min, rinsed with ethanol, heat treated at 120 °C for 1 h, and then dried in air for 12 h. The electrospun nanofibers were then immersed in the growth solution, which was subsequently transferred into a closed, capped glass vial and heated at 90 °C for 8 h. The container was removed from the oven at the end of the reaction period and allowed to reach equilibrium at room temperature for approximately 10−12 h. The treated samples were thoroughly rinsed with DI water and dried in air.

Characterization Methods. The surface morphology of the samples was investigated using a JEOL JSM 6060 LV scanning electron microscope (SEM), in which the samples were coated with a 15 nm layer of gold before observation, and a transmission electron microscope (HRTEM), where the calcined electrospun TiO_2 nanofibers were scraped off the glass slides, dispersed in ethanol solution by sonication, and then mounted on carbon-coated holey Cu grids.

The electrochemical impedance of the samples was measured using a SI 1260 impedance/gain-phase analyzer controlled using the SMaRT software package (operation voltage = 0.5 V, sweep frequency range = 10^7−0.1 Hz). Impedance measurements were performed using a test cell in which the slides containing samples were sandwiched between two circular stainless steel electrodes with an area of 0.5 cm^2.

A Nanovea PS50 3D noncontact profiler with the MountainsMap Premium software was used to measure the arithmetic mean height of the surface along the z-axis (roughness, S_a) and the areal material ratio at a depth of 1 μm below the mean surface (S_{mr}) (ISO 25178). Scans were recorded using an optical pen with a 1 mm resolution. The scan area and step-size were 0.1 × 0.1 mm and 0.1 μm, respectively. Smaller S_a values indicated smoother surfaces.

Thermogravimetric analysis (TGA) and differential scanning calorimetry (DSC) experiments were performed using a Mettler Toledo 851 with a TSO 801RO robotic arm. For the TGA experiments, the samples were heated from 40 to 600 °C at a rate of 10 °C/min under a nitrogen atmosphere at a flow rate of 40 mL/min. For the DSC experiments, the heating rate was set at 10 °C/min in a temperature range from 0 to 550 °C under nitrogen flow. A small amount (approximately 6−10 mg) of the electrospun samples were scraped off the glass slides and analyzed using STARe DBV9.10 software.

The chemical structure of the materials was investigated using a FTIR spectrometer (Avatar 360 FT-IR). The calcined samples were mixed with IR grade KBr and then pelletized for analysis.

RESULTS AND DISCUSSION

The SEM images in Figure 1 reveal that ZnO nanorods can be readily grown on a variety of surfaces using the hydrothermal growth technique, including on the electrospun polystyrene (PS) nanofibers. The electrospun fibers have uniform diameters and smooth surfaces and are randomly oriented on the glass slides. The thickness of the electrospun structures can be varied by changing the electrospinning duration and solution concentrations.

PS was chosen as the "carrier" polymer due to its easy spinnability and miscibility with $Ti(OiPr)_4$. To thoroughly investigate the structure−property relationships of the hierarchical branched TiO_2/ZnO nanostructures, a series of PS/

$Ti(OiPr)_4$ solutions were prepared and the surface properties and charge transfer characteristics were investigated. Table 1 lists the compositions of the electrospinning solutions, weight percentage of TiO_2 in the electrospun PS/TiO_2 samples (determined through thermogravimetric analysis), surface roughness (S_a), areal material ratio (S_{mr}) (1 μm under the mean surface), and the average diameters of the electrospun nanofibers before calcination. The average diameters of the electrospun nanofibers were calculated using the ImageJ program (NIH) by measuring the diameter of 10 random fibers. The S_a and S_{mr} values were calculated using the MountainsMap software on the profiler images.

The $Ti(OiPr)_4$ electrospun in PS nanofibers were rapidly hydrolyzed by the moisture in the air. Without the PS carrier polymer, electrospinning of $Ti(OiPr)_4$ would not be possible. The electrospun fibers were then heated at 120 °C for 1 h to complete the condensation reaction, which generated a uniform and continuous web of TiO_2 nanofibers. Table 1 shows that, before calcination, the diameters of the electrospun fibers decreased with increasing $Ti(OiPr)_4$ ratio. After calcination, which removes the polystyrene carrier polymer, the TiO_2 nanofibers exhibited uniform average diameters of 150 nm, as measured using a series of SEM images. Increasing the amount of $Ti(OiPr)_4$ in the PS solution caused a decrease in the surface roughness of the electrospun fibers. Pure PS fibers are lighter than the TiO_2-containing fibers, which causes them to electrospin more. In addition, the areal material ratios (S_{mr}) were also observed to decrease as the amount of TiO_2 in the PS solution increased, which indicates that the samples were becoming lighter and more voluminous. For example, when pure PS was electrospun, 66.3% of the sample's area was solid material. However, the solution that contained 5 wt % $Ti(OiPr)_4$ had 62.4% of its area as solid material. This finding can be attributed to the generation of smaller nanofibers when the amount of TiO_2 is increased. A higher volume can be beneficial for applications in which active materials need to be transferred into and out of the materials without physical barriers.

For further analysis of the precise ratio of TiO_2 in the electrospun samples, TGA measurements were performed on each sample. All organic compounds, including both PS and solvent, would be removed during the scan, whereas TiO_2 would be left behind. At the end of each scan, the actual amount of TiO_2 produced was determined (Table 1). Figure 2 presents typical TGA curves for the electrospun pure PS and 10 wt % $Ti(OiPr)_4$. The difference in the weight percent losses would indicate the amount of TiO_2 generated in the electrospun nanofibers and consequently provide useful information about the actual composition of the electrospun materials. The PS decomposes in the temperature range of 350−450 °C with a considerable weight loss of the composite, and the weak weight loss below that temperature can be attributed to the adsorbed moisture and/or solvent residues. Figure 3. DSC curves of the nanofibers electrospun (a) from 20 wt % polystyrene solution, (b) from polystyrene solution that initially contained 25 wt % $Ti(OiPr)_4$. Thermal characteristics such as melting temperature, degree of crystallization, and thermal degradation of the electrospun PS and TiO_2 nanofibers were investigated using differential scanning calorimetry (DSC). DSC curves in Figure 3a,b exhibit endothermic peaks

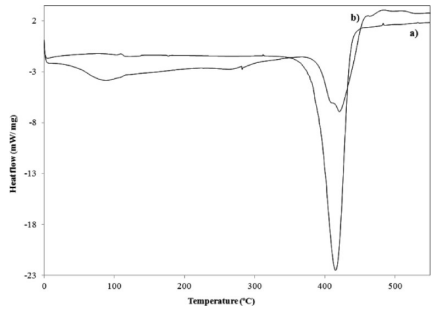

Figure 2. Thermogravimetric analysis of the nanofibers electrospun (a) from 20 wt % polystyrene solution, (b) from polystyrene solution that initially contained 10 wt % $Ti(OiPr)_4$.

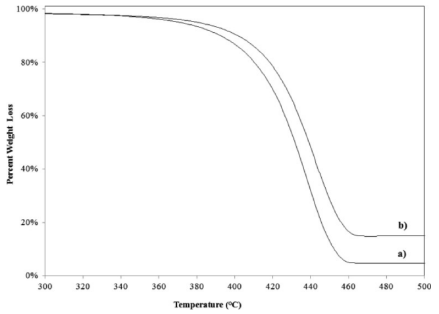

Figure 3. DSC curves of the nanofibers electrospun (a) from 20 wt % polystyrene solution, (b) from polystyrene solution that initially contained 25 wt % $Ti(OiPr)_4$.

in the same temperature range of 350−450 °C that correspond to the decomposition temperature of PS. In Figure 3b, the two exothermic peaks at higher temperature range (450−500 °C) indicate the amorphous-to-crystalline anatase phase transition of the titania precursor.

Figure 4 presents 3D noncontact profiler images of the electrospun nanofibers before calcination. A decrease in average diameter of the nanofibers with increasing $Ti(OiPr)_4$ weight percentage in the spinning solution is clearly observed in these images, and the values are tabulated in Table 1. In addition, these images reveal that the electrospun structures become more porous with increasing amounts of $Ti(OiPr)_4$ in the electrospinning solution. Diameters of the fibers in the micrometer range make the profiler more suitable for this analysis than AFM. Color coding is used to indicate the different heights. A blue to red color change corresponds to the increase in thickness.

Figure 5 presents images of the nanofibers electrospun from PS solution that initially contained 25 wt % $Ti(OiPr)_4$. Highly uniform, continuous, and smooth nanofibers were obtained before (Figure 5a) and after calcination (Figure 5b). Figure 5b, c, and d presents the SEM and HRTEM images of the TiO_2 nanofibers obtained after calcination at 500 °C for 1 h. Calcination of the electrospun nanofibers resulted in a sharp decrease in the average diameter of the nanofibers. Figure 5b is the TEM image of the TiO_2 nanofibers, which shows the continuous formation of TiO_2 metal-oxide. The TiO_2 nanofibers remain intact with uniform diameters and a porous structure, as seen in Figure 5b (inset). Figure 5d shows HRTEM and SAED (inset) images. SAED pattern shows overlapped diffuse rings indicating that the TiO_2 films are polycrystalline that was indexed for anatase TiO_2.

Figure 6 presents the SEM, TEM, and SAED analysis of the ZnO nanorods grown on the electrospun TiO_2 nanofibers.

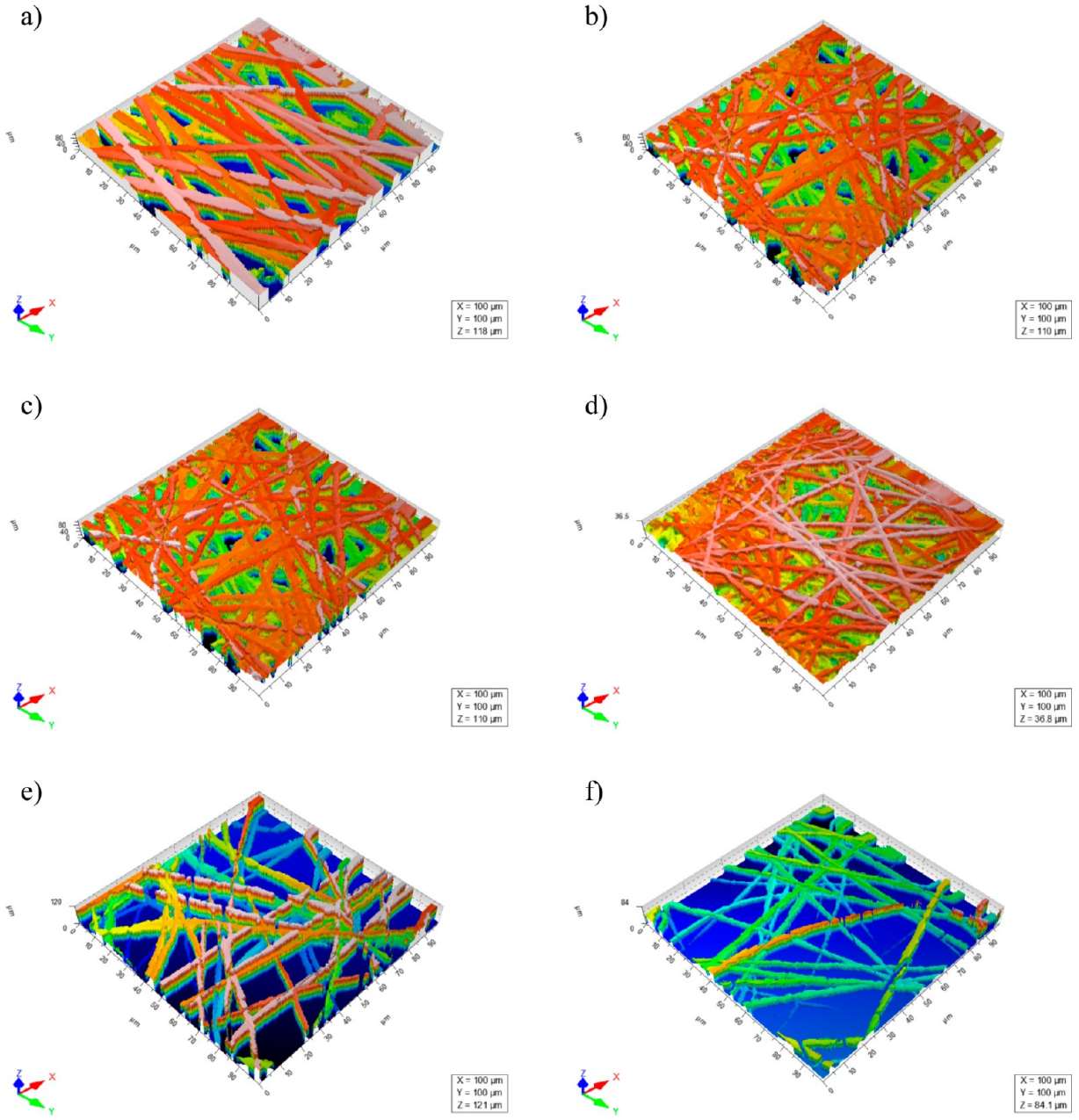

Figure 4. Three-dimensional noncontact profiler images of nanofibers (a) electrospun from 20 wt % polystyrene solution, (b) sample 1, (c) sample 2, (d) sample 3, (e) sample 4, and (f) sample 5.

Figure 6a clearly shows the hexagonal structures of the ZnO nanorods on the electrospun TiO_2 nanofibers. Highly dense, uniform, and radially aligned growth of ZnO nanorods over almost the entire TiO_2 nanofibers can clearly be seen. Figure 6b,d shows the TEM images of the hierarchical nanostructures with ZnO nanorods that have a 70° contact angle with the underlying TiO_2 nanofiber (Supporting Information). The HRTEM image indicates that the nanowires are highly crystalline with a lattice spacing of 0.28 nm, that corresponds to the (0002) planes in the ZnO crystal lattice. The inset in Figure 6c shows a typical selected area electron diffraction (SAED) pattern of the corresponding ZnO nanorods. Together with the HRTEM image, the SAED pattern suggests that the ZnO nanorod growth is along the [0001] direction, the polar *c*-axis of the ZnO crystal lattice, and has the wurtzite crystal structure of ZnO.

Typical synthesis of ZnO follows the controlled hydrolysis of Zn(II)−amine complexes.[72] The amine group acts as a sequestering agent to avoid the spontaneous formation of bulk ZnO precipitates and provide control over the morphology of the ZnO nanostructures in the final materials. Sakohara et al. reported that colloidal stability depends on the amount of acetate groups bound on the surface of ZnO particles that originate from the zinc acetate reagent.[73] In addition, acetate-derived ZnO seeds provide preferential orientation of the *c*-axis.[74] The orientation of the resulting ZnO nanorods was directly determined by the orientation of the seed ZnO nanocrystals. One-dimensional ZnO nanorods can be synthesized owing to facile growth of the wurtzite crystal with the *c*-axis normal to the substrate, which has a hexagonal unit cell with six nonpolar faces capped with polar oxygen and zinc basal planes. The growth rate of various faces can be

dx.doi.org/10.1021/am302061z | *ACS Appl. Mater. Interfaces* 2012, 4, 6917−6926

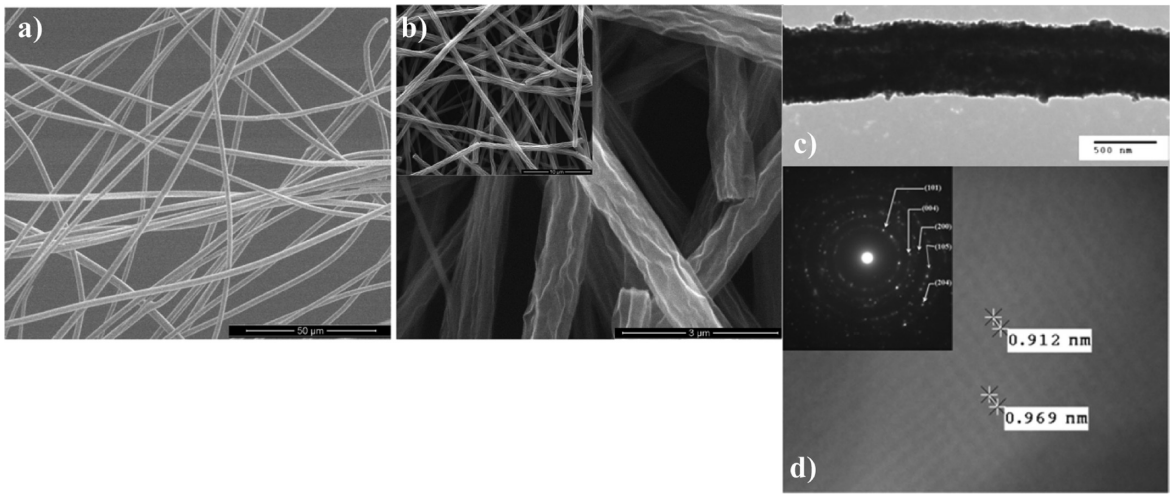

Figure 5. (a) SEM images of the nanofibers electrospun from polystyrene solution that initially contained 25 wt % $Ti(OiPr)_4$, (b) TiO_2 nanofibers generated after calcination at 500 °C (inset: identical sample at low magnification). (c) TEM images and (d) selected area electron diffraction patterns (SAED) and HRTEM lattice micrograph of the TiO_2 nanofibers.

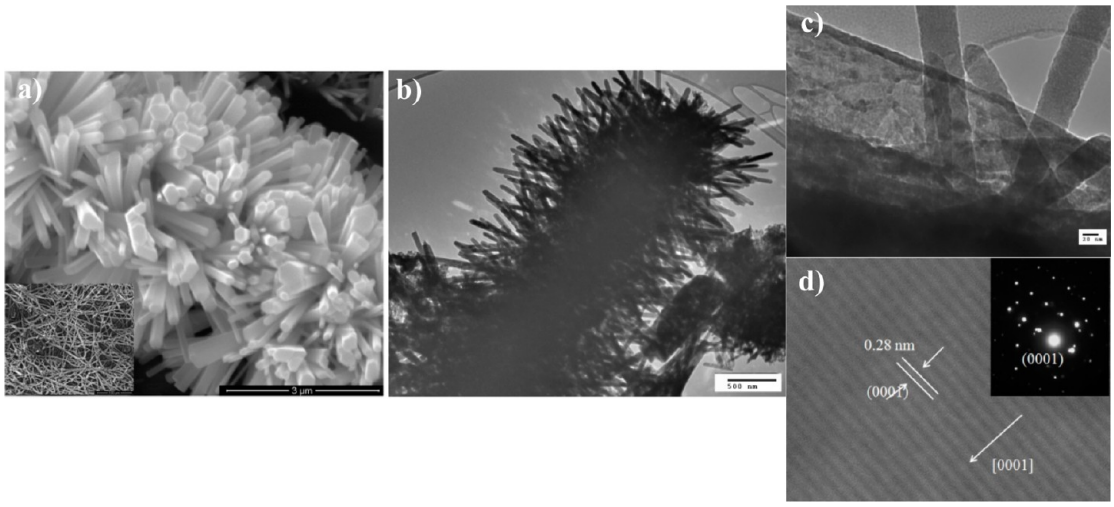

Figure 6. (a) SEM images of the ZnO nanorods grown on the electrospun TiO_2 nanofibers (inset: identical sample at low magnification). (b) TEM images of the ZnO nanorods grown on the electrospun TiO_2 nanofibers. (c) TEM images at higher magnification showing the angle between the ZnO nanorods and the electrospun TiO_2 nanofibers. (d) SAED patterns and HRTEM lattice micrograph of the ZnO nanorods grown on the electrospun TiO_2 nanofibers.

controlled by using additives. Addition of hexamethylenetetramine (HTMA) promotes one-dimensional ZnO precipitation by decomposing during the reaction and increasing the pH for complete hydrolysis of divalent metal ion, Zn(II). Additionally, HTMA can kinetically control species in solution by coordinating to zinc(II) and keeping the free zinc ion concentration low.[75] HMTA can also coordinate to the nonpolar faces of the ZnO crystal that inhibits radial growth but allows axial growth of the nanorods.

Figure 7 shows the branched hierarchical nanostructures of ZnO/TiO_2 at two different magnifications. As seen in Figure 7a–e, the ZnO nanorods were successfully grown on the electrospun TiO_2 nanofibers using a two-step hydrothermal method. Close examination of the branched ZnO nanorods revealed highly dense, radially aligned structures on the TiO_2 nanofibers. The secondary ZnO nanorods have a length ranging from 200 to 400 nm with an average diameter of 80 nm. The growth anisotropy was maintained in the *c*-axis. Seeding was determined to be critical as nucleation sites for the growth of the ZnO nanorods on the TiO_2 nanofibers. The nucleation sites determine the growth kinetics of the secondary ZnO nanorods. There was additional growth of ZnO with various structures, such as flower and dumbbell-like, that were deposited on the sample surface, which made the cleaning process significantly important for obtaining clear images. The dip-coating method, which has been widely used to seed the substrates for subsequent ZnO growth, was particularly problematic. Because the electrospun nanofibers were affixed to a glass slide, they could be easily exfoliated from the surface by the seed solution. Instead, we developed a drop-by-drop soaking method followed by heating at 120 °C for 1 h to ensure durable attachment of the ZnO nanoparticles.

The morphology and density of the secondary ZnO nanorods are strongly dependent on the density of the primary TiO_2 nanofibers, as observed in Figure 7. The ZnO nanorods grown on the electrospun pure PS are needle-like and sparsely distributed over the entire surface (Figure 1). However, a uniform coating of highly dense and low aspect ratio ZnO

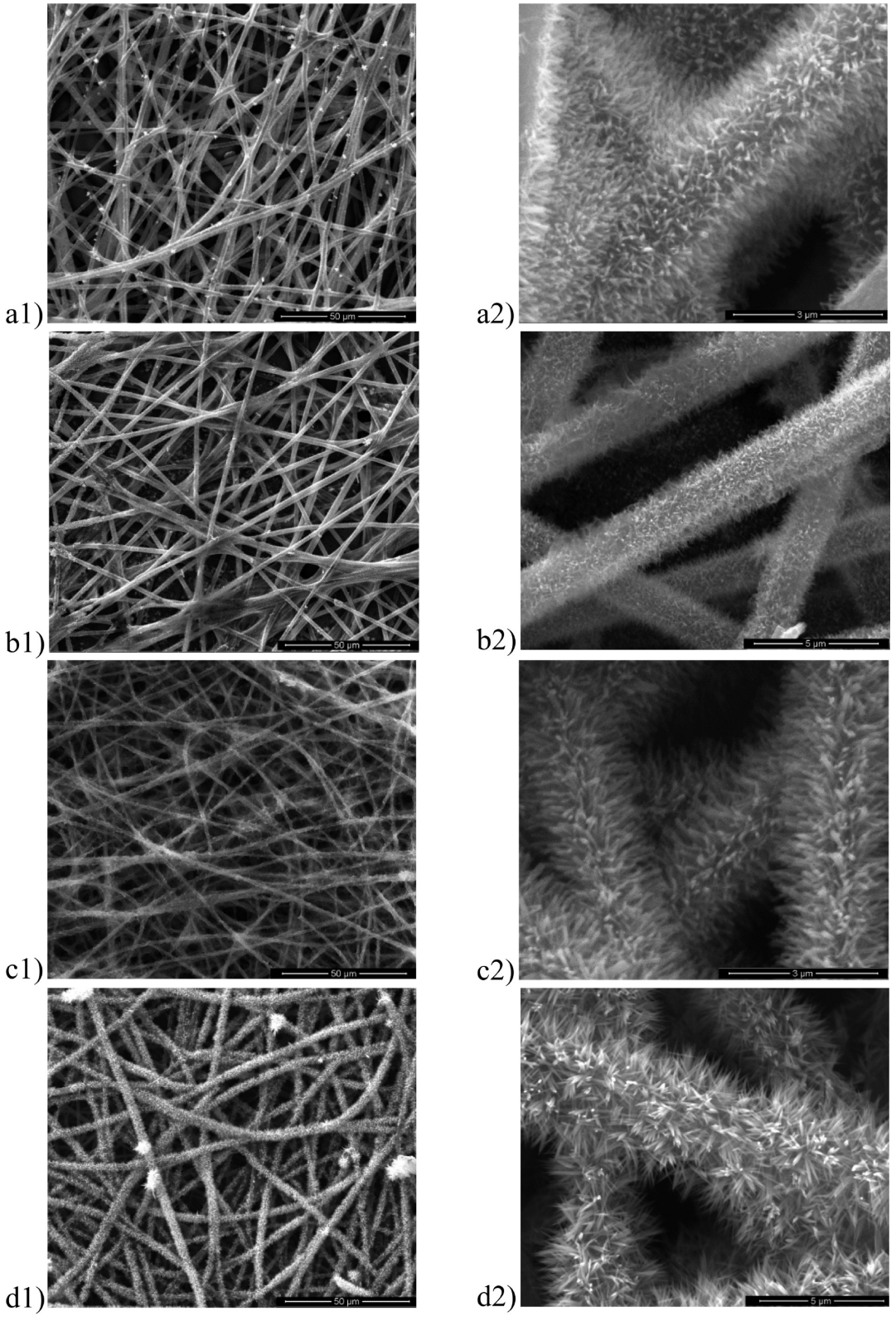

Figure 7. continued

dx.doi.org/10.1021/am302061z | *ACS Appl. Mater. Interfaces* 2012, 4, 6917−6926

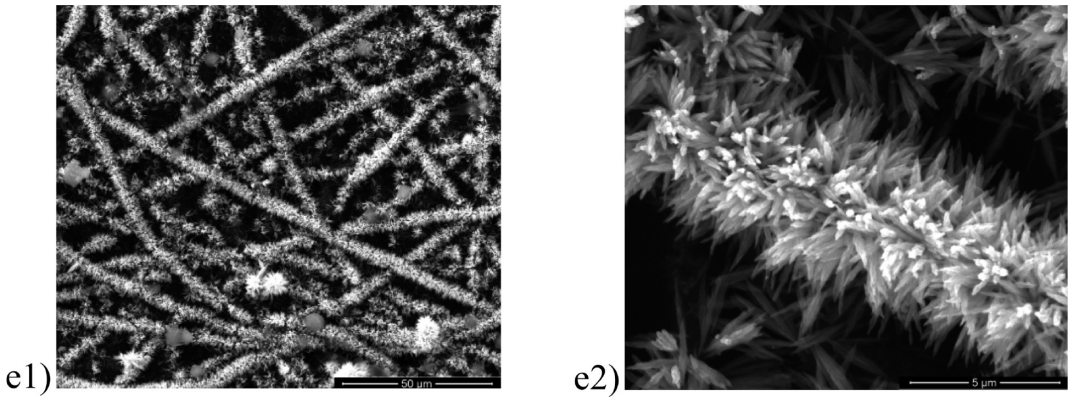

Figure 7. SEM images of (a1−a2) sample 1, (b1−b2) sample 2, (c1−c2) sample 3, (d1−d2) sample 4, and (e1−e2) sample 5.

nanorods was observed on the electrospun TiO_2 nanofibers. As the density of TiO_2 increases, ZnO nanorods with a dense and overlapping morphology are observed. The TiO_2 surface appears to be promoting the growth of the ZnO nanorods.

Figure 8 presents the infrared spectral region between 400 and 3900 cm^{-1} of the calcined TiO_2 nanofibers (electrospun

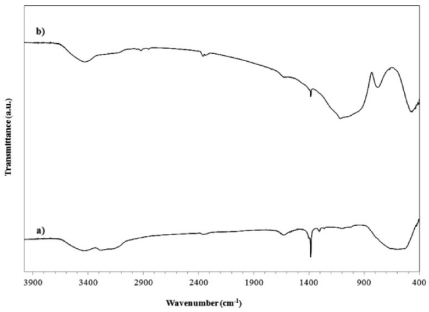

Figure 8. FTIR spectra of (a) the TiO_2 nanofibers obtained from calcination of the electrospun polystyrene that initially contained 25 wt % $Ti(OiPr)_4$; (b) ZnO nanorods grown on the TiO_2 nanofibers.

from PS solution containing 25 wt % $Ti(OiPr)_4$) with and without the ZnO nanorods. The hydroxyl groups in Ti−OH are observed as a broad absorption band in the range of ∼3500−3000 cm^{-1} in the hydrolyzed TiO_2 precursor, as shown in Figure 8a. In the low-energy interval, the stretching vibration band of Ti−O−Ti is observed at approximately 600 cm^{-1}. The presence of these bands indicates that the hydrolysis (Ti−OR → Ti−OH) and condensation (Ti−OH + Ti−OR (or Ti−OH) → Ti−O−Ti) reactions of $Ti(OiPr)_4$ take place. The IR spectrum of the sample that contains ZnO nanorods on identical electrospun TiO_2 nanofibers is shown in Figure 8b. The band at 440 cm^{-1} is attributed to the Zn−O vibration. The peak at 3450 cm^{-1} indicates the presence of OH groups. The band around 1100 cm^{-1} is ascribed to the overlapping peaks of the vibrations of methyl groups of the tetramethyleneamine and of C−O groups. Although the Zn−O vibration band shifts to higher wavenumbers, the broad band of the Ti−O−Ti stretching vibration at approximately 600 cm^{-1} disappears, which indicates that the ZnO nanorods affect the surface of TiO_2.[76]

The ac impedance technique measures the resistance of the surface to current flow when a voltage is applied. The results are presented in complex impedance plane plots (also known as Nyquist plots), in which the real part is plotted against the imaginary part of the impedance. The distinctive semicircle in the high-frequency region represents the interfacial resistance of the material to electron transfer. The electron transfer resistance (R_{CT}) is equal to the diameter of the semicircle, which controls the electron transfer kinetics. The straight line appearing after the semicircle in the low-frequency region represents the Warburg impedance, and it is caused by the diffusion of ions at the interface (mass transfer). When the slope of the impedance, which represents mass transfer, approaches an ideal straight line, it implies enhanced accessibility of the ions and/or possible contributions of pseudocapacitance. Figure 9 presents the dependence of the ac

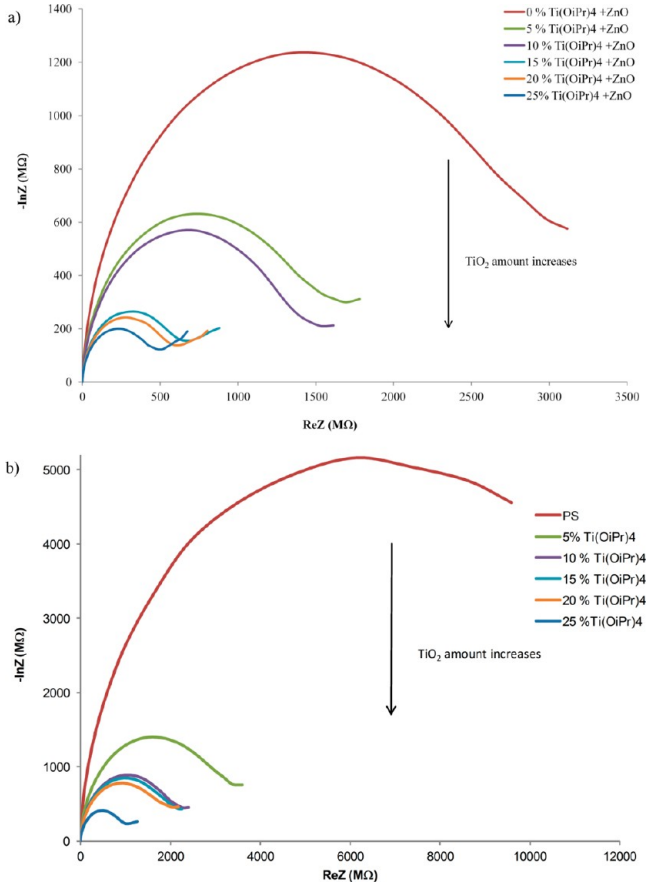

Figure 9. Electrochemical impedance spectra of (a) TiO_2 nanofibers obtained from calcination of the electrospun polystyrene solutions with increasing amount of $Ti(OiPr)_4$.

dx.doi.org/10.1021/am302061z | ACS Appl. Mater. Interfaces 2012, 4, 6917−6926

impedance on the density of the TiO_2 in the electrospun fibers with and without ZnO nanorods. With increasing TiO_2 concentration, the diameters of the semicircles (R_{CT}) sharply decrease, which indicates low interfacial resistance in the system (Figure 9a). As expected, increasing the amount of TiO_2 improved the interfacial conductivity. The electron transfer was further enhanced by the formation of the branched hierarchical ZnO nanorods/TiO_2 nanofiber system (Figure 9b). The coupling of two semiconductors, with one functioning as an electron donor and the other as an acceptor, facilitates the dissociation of excitons at the donor–acceptor interface due to the difference in band gaps. Therefore, the presence of efficient interfaces as ordered heterojunctions is of paramount importance for more effective exciton dissociation.

The conduction band of ZnO lies at a more negative potential than that of TiO_2, whereas the valence band of TiO_2 is more positive than that of ZnO. When an appropriate energy is applied, mobilized electrons can easily jump from the conduction band of ZnO to the corresponding band of TiO_2, and hole transfer occurs from the valence band of TiO_2 to that of ZnO. The simultaneous transfer of electrons and holes in the ZnO–TiO_2 system should increase both the yield and the lifetime of charge carriers (Figure 10). The large aspect ratio and the directional mobility of charge carriers in nanorod systems are the primary contributors to the greater mobility of charge carriers.[50]

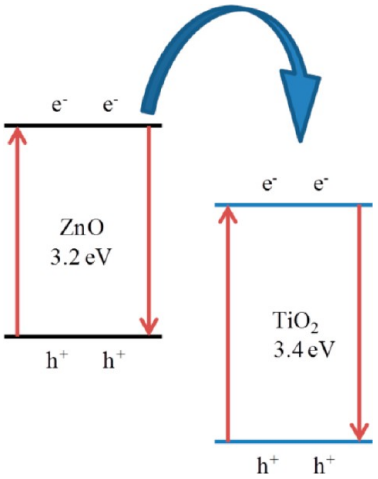

Figure 10. Schematic diagram of energy band matching and electron–hole separations of ZnO–TiO_2 systems.

CONCLUSIONS

In this study, we have demonstrated that the combination of electrospinning and hydrothermal growth techniques results in robust and unique branched hierarchical metal-oxide nanoheterostructures with improved electronic properties. The morphologies of the ZnO nanorods were demonstrated to be dependent on the density of the underlying TiO_2 nanofibers. The electrospun TiO_2 nanostructures are highly porous, which can play an important role when the easy penetration of active materials is required, such as for electrolytes in solar cell applications. Electrospinning combined with the hydrothermal growth methodology can also be applied to the development of various combinations of metal-oxide nanoheterostructures for applications in photocatalysis, photovoltaics, and sensing.

ASSOCIATED CONTENT

Supporting Information

Additional figure. This material is available free of charge via the Internet at http://pubs.acs.org.

AUTHOR INFORMATION

Corresponding Author

*E-mail: ruya-ozer@utulsa.edu. Telephone: 918-631-3028.

Notes

The authors declare no competing financial interest.

ACKNOWLEDGMENTS

We would like to thank the Department of Chemistry & Biochemistry at The University of Tulsa for its support. We greatly appreciate the financial support from The University of Tulsa Institute of Nanotechnology, TU Student Research Grants Program, and the Faculty Development Summer Fellowship and Research Programs for financial support. We would also like to thank Mr. Rick Portman for his help with SEM analyses. We acknowledge Mr. Terry Colberg of Oklahoma State University, Electron Microscopy Lab, for help with obtaining the TEM and SAED images.

REFERENCES

(1) Xiong, Q.; Grimes, C. A.; Zacharias, M.; Fontcuberta i Morral, A.; Hiruma, K.; Shen, G. *J. Nanotechnol.* **2012**, special issue.
(2) Lieber, C. M. *MRS Bull.* **2011**, *36*, 1052–1063.
(3) Lauhon, L.; Gudiksen, M.; Wang, D.; Lieber, C. *Nature* **2002**, *420*, 57–61.
(4) Hayden, O.; Agarwal, R.; Lu, W. *Nano Today* **2008**, *3*, 12–22.
(5) Wu, Y.; Yan, H.; Huang, M.; Messer, B.; Song, J. H.; Yang, P. *Chem.—Eur. J.* **2002**, *8*, 1260–1268.
(6) Xia, Y.; Yang, P.; Sun, Y.; Wu, Y.; Mayers, B.; Gates, B.; Yin, Y.; Kim, F.; Yan, H. *Adv. Mater.* **2003**, *15*, 353–389.
(7) Zhai, T.; Fang, X.; Liao, M.; Xu, X.; Zeng, H.; Yoshio, B.; Golberg, D. *Sensors* **2009**, *9*, 6504–6529.
(8) Bierman, M. J.; Jin, S. *Energy Environ Sci.* **2009**, *2*, 1050–1059.
(9) Agarwal, R. *Small* **2008**, *4*, 1872–1893.
(10) Lao, J. Y.; Wen, J. G.; Ren, Z. F. *Nano Lett.* **2002**, *2*, 1287–1291.
(11) Wang, Z.; Pan, Z. *Adv. Mater.* **2002**, *245*, 1029–1032.
(12) Jiang, X.; Tian, B.; Xiang, J.; Zeng, G.; Wang, H.; Mai, L.; Lieber, C. *Proc. Natl. Acad. Sci. U.S.A.* **2011**, *108*, 12212–12216.
(13) Wang, D.; Qian, F.; Yang, C.; Zhong, Z.; Lieber, C. M. *Nano Lett.* **2004**, *4*, 871–874.
(14) Mieszawska, A. J.; Jalilian, R.; Sumanasekera, G. U.; Zamborini, F. P. *Small* **2007**, *3*, 722–756.
(15) Jung, Y.; Ko, D.-K.; Agarwal, R. *Nano Lett.* **2007**, *7*, 264–268.
(16) Sahay, R.; Kumar, P. S.; Sridhar, R.; Sundaramurthy, J.; Venugopal, J.; Mhaisalkar, S. G.; Ramakrishna, S. *J. Mater. Chem.* **2012**, *22*, 12953–12971.
(17) Agarwal, S.; Greiner, A.; Wendorff, J. H. *Adv. Funct. Mater.* **2009**, *19*, 2863–2879.
(18) Agarwal, S.; Wendorff, J. H.; Greiner, A. *Macromol. Rapid Commun.* **2010**, *31*, 1317–1331.
(19) Ramakrishna, S.; Fujihara, K.; Teo, W.-E.; Lim, T.-C.; Ma, Z. *An Introduction to Electrospinning and Nanofibers*; World Scientific: Singapore, 2005
(20) Dai, Y.; Liu, W.; Formo, E.; Sun, Y.; Xia, Y. *Polym. Adv. Technol.* **2011**, *22*, 326–338.
(21) Chronakis, I. *J. Mater. Process. Technol.* **2005**, *167*, 283–293.
(22) Sigmund, W.; Yuh, J.; Park, H.; Maneeratana, V.; Pyrgiotakis, G.; Daga, A.; Taylor, J.; Nino, J. C. *J. Am. Ceram. Soc.* **2006**, *89*, 395–407.
(23) Reneker, D. H.; Yarin, A. L. *Polymer* **2008**, *49*, 2387–2425.
(24) Teo, W.; Inai, R.; Ramakrishna, S. *Sci. Technol. Adv. Mater.* **2011**, *12*, 013002.

(25) Greiner, A.; Wendorff, J. H. *Angew. Chem., Int. Ed.* **2007**, *46*, 5670−5703.
(26) Miao, J.; Miyauchi, M.; Simmons, T. J.; Dordick, J. S.; Linhardt, R. J. *J. Nanosci. Nanotechnol.* **2010**, *10*, 5507−5519.
(27) Lu, X.; Wang, C.; Wei, Y. *Small* **2009**, *5*, 2349−2370.
(28) Tiano, A. L.; Koenigsmann, C.; Santulli, A. C.; Wong, S. S. *Chem. Commun.* **2010**, *46*, 8093−8130.
(29) Chigome, S.; Torto, N. *Anal. Chim. Acta* **2011**, *706*, 25−36.
(30) Dong, Z.; Kennedy, S. J.; Wu, Y. *J. Power Sources* **2011**, *196*, 4886−4904.
(31) Huang, Z. M.; Zhang, Y. Z.; Kotaki, M.; Ramakrishna, S. *Compos. Sci. Technol.* **2003**, *63*, 2223−2253.
(32) Reneker, D. H.; Chun, I. *Nanotechnology* **1996**, *7*, 216−223.
(33) Frenot, A.; Chronakis, I. S. *Curr. Opin. Colloid Interface Sci.* **2003**, *8*, 64−75.
(34) Yuh, J.; Perez, L.; Sigmund, W. M.; Nino, J. C. *J. Sol−Gel Sci. Technol.* **2007**, *42*, 323−329.
(35) Ren, H.; Ding, Y.; Jiang, Y.; Xu, F.; Long, Z.; Zhang, P. *J. Sol−Gel Sci. Technol.* **2009**, *52*, 287−290.
(36) Cai, Z.; Song, J.; Li, J.; Zhao, F.; Luo, X.; Tang, X. *J. Sol-Gel Sci. Technol.* **2011**, *61*, 49−55.
(37) Evcin, A.; Kaya, D. A. *Sci. Res. Essays* **2010**, *5*, 3682−3686.
(38) Starbova, K.; Petrov, D.; Starbov, N.; Lovchinov, V. *Ceram. Int.* **2012**, *8*, 4645−4651.
(39) Dai, H.; Gong, J.; Kim, H.; Lee, D. *Nanotechnology* **2002**, *13*, 674−677.
(40) Ramaseshan, R.; Sundarrajan, S.; Jose, R.; Ramakrishna, S. *J. Appl. Phys.* **2007**, *102*, 111101.
(41) Chuangchote, S.; Sagawa, T.; Yoshikawa, S. *J. Mater. Res.* **2011**, *26*, 2316−2321.
(42) Chuangchote, S.; Sagawa, T.; Yoshikawa, S. *J. Appl. Polym. Sci.* **2009**, *114*, 2777−2791.
(43) Formo, E.; Lee, E.; Campbell, D.; Xia, Y. *Nano Lett.* **2008**, *8*, 668−672.
(44) Bao, N.; Li, Y.; Wei, Z.; Yin, G.; Niu, J. *J. Phys. Chem. C* **2011**, *115*, 5708−5719.
(45) Choi, S.; Kim, S.; Lim, S.; Park, H. *J. Phys. Chem. C* **2010**, *114*, 16475−16480.
(46) Ganesh, V. A.; Nair, A. S.; Raut, H. K.; Walsh, T. M.; Ramakrishna, S. *RSC Adv.* **2012**, *2*, 2067−2072.
(47) Archana, P.; Jose, R.; Vijila, C. *J. Phys. Chem. C* **2009**, *113*, 21538−21542.
(48) Wang, L.; Kang, Y.; Wang, Y.; Zhu, B.; Zhang, S.; Huang, W.; Wang, S. *Mater. Sci. Eng., C* **2012**, *32*, 2079−2085.
(49) Lin, D.; Wu, H.; Zhang, R.; Zhang, W.; Pan, W. *J. Am. Ceram. Soc.* **2010**, *93*, 3384−3389.
(50) Shang, M.; Wang, W.; Yin, W.; Ren, J.; Sun, S.; Zhang, L. *Chem.—Eur. J.* **2010**, *16*, 11412−11419.
(51) Soldano, C.; Comini, E.; Baratto, C.; Ferroni, M.; Faglia, G.; Sberveglieri, G. *J. Am. Ceram. Soc.* **2012**, *20*, 1−20.
(52) Meixner, H.; Gerblinger, J.; Lampe, U. *Sensors* **2009**, *9*, 9903−9924.
(53) Park, J. Y.; Choi, S.-W.; Lee, J.-W.; Lee, C.; Kim, S. S. *J. Am. Ceram. Soc.* **2009**, *92*, 2551−2554.
(54) Zhang, Z.; Shao, C.; Li, X.; Zhang, L. *J. Phys. Chem. C* **2010**, *114*, 7920−7925.
(55) Liu, R.; Ye, H.; Xiong, X.; Liu, H. *Mater. Chem. Phys.* **2010**, *121*, 432−439.
(56) Kanjwal, M. A.; Barakat, N. A. M.; Sheikh, F. A.; Kim, H. Y. *Bioceramics Development and Applications* **2011**, *1*, 1−3.
(57) Kanjwal, M. A.; Barakat, N. A. M.; Sheikh, F. A.; Park, D. K.; Kim, H. Y. *J. Mater. Sci.* **2010**, *45*, 3833−3840.
(58) Wang, Z.; Li, Z.; Sun, J.; Zhang, H. *J. Phys. Chem. C* **2010**, *114*, 6100−6105.
(59) Mu, J.; Chen, B.; Zhang, M.; Guo, Z.; Zhang, P.; Zhang, Z.; Sun, Y.; Shao, C.; Liu, Y. *ACS Appl. Mater. Interfaces* **2012**, *4*, 424−430.
(60) Su, C.; Shao, C.; Liu, Y. *J. Colloid Interface Sci.* **2011**, *359*, 220−227.
(61) Zhang, Z.; Shao, C.; Li, X.; Wang, C.; Zhang, M.; Liu, Y. *ACS Appl. Mater. Interfaces* **2010**, *2*, 2915−2923.
(62) Kanjwal, M. A.; Sheikh, F. A.; Barakat, N. A. M.; Li, X.; Kim, H. Y.; Chronakis, I. S. *Appl. Surf. Sci.* **2012**, *258*, 3695−3702.
(63) Kanjwal, M. A.; Barakat, N. A. M.; Sheikh, F. A.; Park, S. J.; Kim, H. Y. *Macromol. Res.* **2010**, *18*, 233−240.
(64) Ostermann, R.; Li, D.; Yin, Y.; McCann, J. T.; Xia, Y. *Nano Lett.* **2006**, *6*, 1297−1302.
(65) Wang, C.; Shao, C.; Zhang, X.; Liu, Y. *Inorg. Chem.* **2009**, *48*, 7261−7268.
(66) Sun, C.; Wang, N.; Zhou, S.; Hu, X.; Zhou, S.; Chen, P. *Chem. Commun.* **2008**, 3293−3295.
(67) Vayssieres, L.; Keis, K.; Lindquist, S. *J. Phys. Chem. B* **2001**, *28*, 3350−3352.
(68) Hari, P.; Spencer, D. *Phys. Status Solidi C* **2009**, *6*, S150−S153.
(69) AbuDakka, M.; Qurashi, A.; Hari, P.; Wakas Alam, M. *Mater. Sci. Semicond. Proc.* **2010**, *13*, 115−118.
(70) Hari, P.; Spencer, D.; Hor, A.; Liang, H.; Roberts, K.; Teeters, D. *Phys. Status Solidi C* **2011**, *8*, 2814−2817.
(71) Athauda, T. J.; Butt, U.; Ozer, R. R. *MRS Proc.* **2012**, DOI: 10.1557/opl.2012.844.
(72) Baruah, S.; Thanachayanont, C.; Dutta, J. *Sci. Technol. Adv. Mater.* **2008**, *9*, 025009.
(73) Sakohara, S.; Ishida, M.; Anderson, M. A. *J. Phys. Chem. B* **1998**, *102*, 10169−10175.
(74) Greene, L. E.; Law, M.; Tan, D. H.; Montano, M.; Goldberger, J.; Somorjai, G.; Yang, P. *Nano Lett.* **2005**, *5*, 1231−1236.
(75) Greene, L. E.; Yuhas, B. D.; Law, M.; Zitoun, D.; Yang, P. *Inorg. Chem.* **2006**, *45*, 7535−7543.
(76) Bahadur, N. M.; Furusawa, T.; Sato, M.; Kurayama, F.; Suzuki, N. *Mater. Res. Bull.* **2010**, *45*, 1383−1388.